Enhanced output power using MgZnO/ZnO/MgZnO double heterostructure in ZnO homojunction light emitting diode

Sheng Chu,[1] Jianze Zhao,[1,2] Zheng Zuo,[1] Jieying Kong,[1] Lin Li,[1] and Jianlin Liu[1,a)]
[1]*Quantum Structures Laboratory, Department of Electrical Engineering, University of California at Riverside, Riverside, California 92521, USA*
[2]*School of Physics and Optoelectronic Engineering, Dalian University of Technology, Dalian, 116024 China*

(Received 9 December 2010; accepted 10 May 2011; published online 23 June 2011)

A diode with Sb-doped *p*-type ZnO, MgZnO/ZnO/MgZnO double heterostructure, and undoped *n*-type ZnO layers was grown on *c*-plane sapphire substrate by plasma-assisted molecular-beam epitaxy. Hall effect measurement showed that the top *p*-type Sb-doped ZnO layer has a hole concentration of $1 \times 10^{17} cm^{-3}$. Mesa geometry light emitting diodes were fabricated with Au/Ni and Au/Ti Ohmic contacts on top of the *p*-type and *n*-type layers, respectively. Ultraviolet emission was achieved, which yielded an output power of 457 nW at 140 mA. The enhancement of the output power is attributed to carrier confinement in the good-quality intrinsic layer of the double heterostructure. The spatial distribution of light emission was characterized. © *2011 American Institute of Physics*. [doi:10.1063/1.3598136]

I. INTRODUCTION

ZnO is promising for ultraviolet optoelectronic devices due to its large exciton binding energy (60 meV) and suitable bandgap (3.37 eV).[1,2] In order to achieve applicable ZnO devices, much progress has been made on *p*-type doping of ZnO films and nanostructures.[3–6] Among these efforts, Sb doping for *p*-type ZnO was theoretically proposed and experimentally confirmed subsequently.[7,8] Various functional prototype devices such as photodetectors,[9,10] light-emitting diodes (LEDs),[11–13] and random lasing devices[14] based on Sb-doped ZnO have been demonstrated, indicating that Sb can be an effective *p*-type dopant for ZnO. However, the best output power previously obtained in LED with Sb-doped *p*-type ZnO on *c*-plane sapphire substrate was only 32 nW,[15] which is possibly due to the low doping level and insufficient structural engineering. To increase the output power, improved *p*-type film and double heterostructure may be used. In this study, Sb-ZnO/MgZnO/ZnO/MgZnO/ZnO double heterostructure LEDs on *c*-plane sapphire substrates with greatly improved output power of 287 nW at 60 mA and 457 nW at 140 mA are reported.

II. DEVICE GROWTH AND FABRICATION

The double heterostructure diode was grown on *c*-plane sapphire substrates using plasma-assisted molecular-beam epitaxy (MBE). Sapphire substrates were chemically cleaned in an aqua regia (HNO_3: HCl = 1:3) solution at 150 °C for 20 min, then rinsed in de-ionized water, and finally dried with a nitrogen gun and transferred into an MBE chamber. The growth began with a 2-min growth of MgO for improving the subsequent ZnO film quality,[16] followed by a regular ZnO buffer layer growth at 550 °C for 8 min. The subsequent *n*-ZnO and Sb-doped *p*-type layers were grown at 700 °C and 500 °C, respectively. The effusion cell temperatures of Zn, Mg, and Sb were 365, 380, and 370 °C, respectively. The Zn and Mg beam fluxes were on the order of 10^{-7} Torr, while Sb beam flux was on the order of 10^{-9} Torr. The *n*-type ZnO and ZnO buffer layers were grown under near stoichiometric condition while the Sb-doped ZnO layer was grown under oxygen rich condition. The thickness of the buffer, *n*-type ZnO, and Sb-doped *p*-type ZnO layers are ∼10, ∼400, and ∼400 nm, respectively. Between the *p*-type and *n*-type layers, a 20 nm MgZnO/∼80 nm undoped ZnO/20 nm MgZnO double heterostructure was inserted as the active region, and the growth temperature of this layer was 400 °C. The mole fraction of Mg in MgZnO was designed to be 10%. Post growth thermal annealing was performed at 750 °C in oxygen ambient to activate the dopants. Mesa geometry LEDs of $800 \times 800\ \mu m^2$ were fabricated using standard photolithography and lift-off processes. Au/Ti and Au/Ni were deposited on *n*-type ZnO layer and Sb-doped *p*-type layer, respectively, as electrical contacts using e-beam evaporation. Ohmic contacts were achieved after rapid thermal annealing process. Figure 1(a) shows the schematic of the device structure. Secondary ion mass spectroscopy (SIMS) measurements were performed by a Cameca IMS 4.5 F system, and the result is shown in Fig. 1(b). The SIMS spectra show the profile of elements O, Zn, Sb, and Mg along the growth direction. The elemental distribution is consistent with the designed device structure. The Sb and Mg diffusion is probably due to the high temperature annealing after growth.

III. RESULTS AND DISCUSSION

X-ray diffraction (XRD) $\theta/2\theta$ survey shows that the diode film grows preferentially along the *c*-direction of the ZnO wurtzite lattice [Fig. 2(a)]. Surface morphology and cross section of the ZnO film were studied by scanning electron microscope (SEM). Figure 2(b) shows the top-view image of the ZnO film on sapphire substrate. It is evident

[a)]Author to whom correspondence should be addressed. Electronic mail: jianlin@ee.ucr.edu.

 © 2011 American Institute of Physics

Author complimentary copy. Redistribution subject to AIP license or copyright, see http://jap.aip.org/jap/copyright.jsp

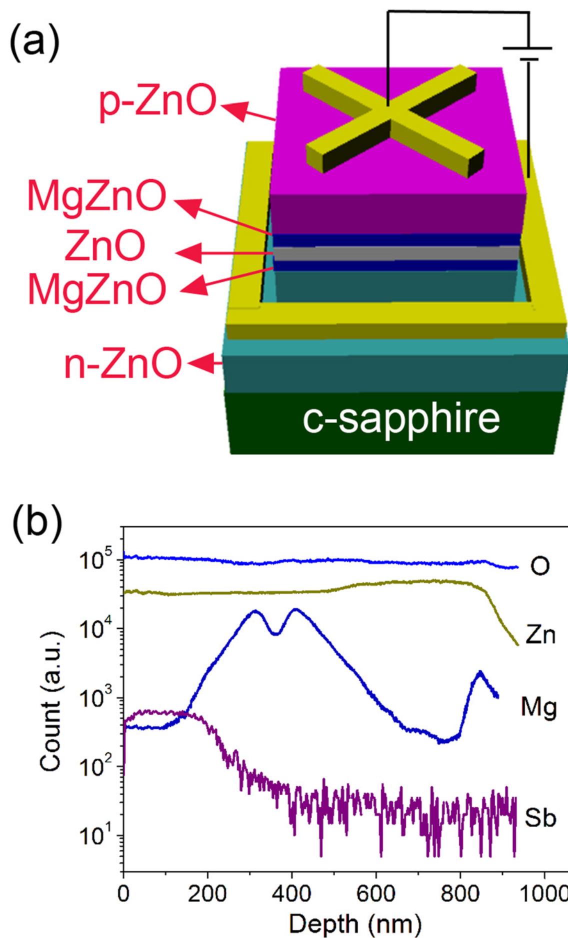

FIG. 1. (Color online) (a) Schematic of the ZnO LED showing a MgZnO/ZnO/MgZnO double heterojunction sandwiched between *p*-type and *n*-type layers. Device mesa with Au/Ni and Au/Ti Ohmic contacts are also shown. (b) SIMS spectra of Zn, O, Mg, and Sb elemental distribution.

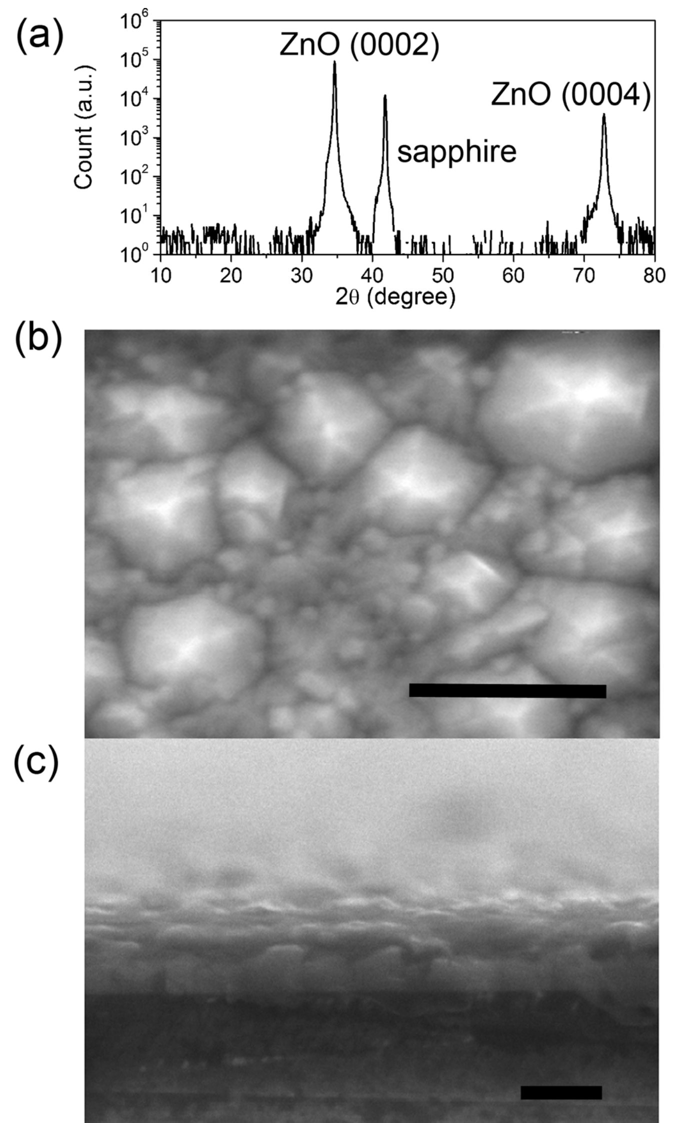

FIG. 2. (a) XRD pattern of the double heterojunction sample. (b) Top-view SEM image of the sample surface. Scale bar: 500 nm (c) Side-view SEM image of the cross-section of the sample. Scale bar: 500 nm. Contrast between *p*-type layer and *n*-type layer is clearly observed.

that ZnO grains with in-plane size from 200 to 500 nm are formed, which is a typical result of oriented nucleation process due to the large lattice mismatch between ZnO and *c*-sapphire substrate. Figure 2(c) shows the cross-sectional SEM image of the film, which confirms the nanocolumnar grain growth mode. In addition, there is evident contrast between the top *p*-type layer and bottom *n*-type layer, which is a result of different growth temperature as well as extensive Sb dopant incorporation in the top film.

Hall effect measurement was characterized under a Hall bar configuration at room temperature. The sample was cut into $\sim$15 mm $\times$ 5 mm bar with Au/Ni Ohmic contacts on both ends and sides. The hole concentration of 1×10^{17} cm^{-3}, mobility of 17 cm^2/V s, and resistivity of 3.6 Ω cm were obtained by linear fitting the Hall resistance with magnetic field. It should be noted that the electrical properties of the *p*-type ZnO layer can be extracted in a multilayer structure for the first time. This might have something to do with the MgZnO/ZnO/MgZnO double heterostructure, which acts as the space charge region of the diode and effectively suppresses the effect from the underlying *n*-ZnO layer. In order to cross-check the carrier concentration of the *p*-type layer, a reference sample with the *n*-type ZnO film only was grown under the same growth condition. The electron concentration, mobility and resistivity of this sample are 5.0×10^{17}/cm^3, 23.2 cm^2/V s and 0.5 Ω cm, respectively. Capacitance-voltage (C-V) analysis (see Fig. S1 in supplemental materials[17]) under standard diode model was performed and yielded a doping concentration of 6.0×10^{16}/cm^3 in the *p*-type layer. This result slightly deviates but is in reasonable agreement with the hole concentration deduced from the Hall effect measurement.

Electrical properties of the LED devices were characterized by Agilent B 1500 A semiconductor parameter analyzer. Figure 3 shows the current-voltage (I-V) characteristic of a ZnO diode device, suggesting typical diode rectifying characteristic. The inset in Fig. 3 shows the linear I-V curves of *n*–*n* contacts on undoped ZnO layer and *p*–*p* contacts on Sb-doped ZnO layer, respectively, indicating the formation of Ohmic contacts. The Ohmic behavior of metal contacts on top of ZnO excludes the possibility of metal-semiconductor junctions in the device.

Author complimentary copy. Redistribution subject to AIP license or copyright, see http://jap.aip.org/jap/copyright.jsp

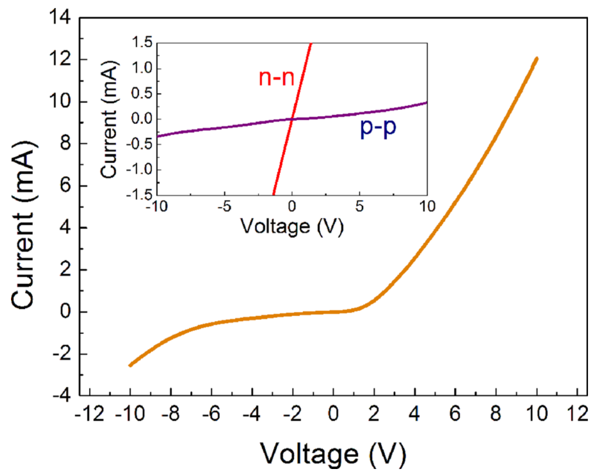

FIG. 3. (Color online) I-V characteristic in linear scale of the device, showing typical rectifying diode characteristic. The inset shows the I-V for contacts on *p*-type layer and *n*-type layer, respectively.

Electroluminescence (EL) characterizations were performed by using a home-built measurement setup including an Oriel monochromator and a lock-in amplifier with a chopper. An external HP E3630 A dc power supply was used to input current to the diodes. Figure 4 shows the EL spectra of the LED device at the injected currents ranging from 30 to 70 mA. The near-bandedge (NBE) ultraviolet emissions are present in the EL spectra and the emission intensity increases with the increase of the injection current. The EL peak position redshifts from 3.26 eV (380 nm) at small injection current (20 mA) to 3.06 eV (405 nm) at large injection current (70 mA), which is attributed to heat induced bandgap shrinkage.[12] The output power of the device was measured and calibrated with an Ocean-Optics integral sphere and an Ocean-Optics LS-CAL-1 standard lamp. Well defined emission signal can be observed and the output power of this device is calculated to be 457 nW (140 mA). The top inset of Fig. 4 shows the image of the emitting light of the device on a TO5 can at the injection current of 140 mA, which was captured by a photocamera. Referring to the device structure shown in Fig. 1(a), it is obvious that the ultraviolet/blue lighting area covers the whole square-shaped mesa area, indicating that the light originates from the planar ZnO *p*-*n* junction. The integrated intensity against injection current is shown in the bottom inset of Fig. 4, suggesting quasilinear relationship between output power and injection current, which is a typical LED characteristic. As a result, the output power is estimated to be 287 nW at the injection current of 60 mA. This value is almost one order of magnitude larger than the previously reported Sb–ZnO/Ga–ZnO junction LED with the same size of $800 \times 800\ \mu m^2$ on *c*-sapphire (32 nW output at the same current of 60 mA).[15]

The spatial distribution of the light emission was characterized by angle-dependent EL measurement. The measurement was achieved by rotating the device sample holder with respect to the growth direction of the sample, as schematically shown in the inset of Fig. 5(a). The EL spectra for 0°, 30°, 45°, 60°, and 90° are shown in Fig. 5(a). Clearly, similar UV emissions are demonstrated at all the five angles, which indicate that this device has fairly broad emission that covers the whole semi-sphere. The broad emission profile in this device is related to the textured surface [as shown in Fig. 2(b)], which enhances the light output due to the reduction of internal reflection in the ZnO/air interface.[18] It is also noticeable

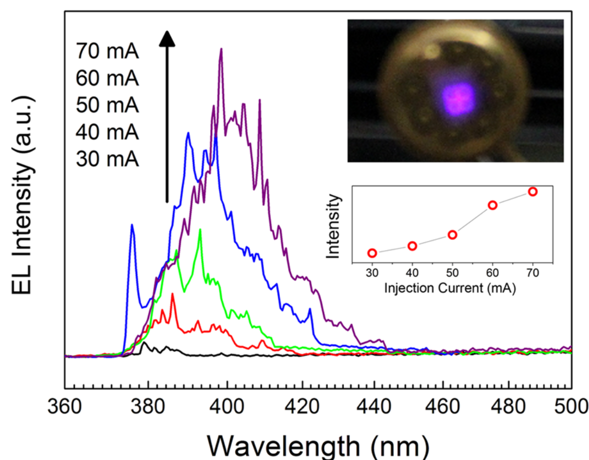

FIG. 4. (Color online) EL spectra at the injection currents ranging from 30 to 70 mA. Top inset: a photo of the LED operating at 140 mA. Bottom inset: integrated spectrum intensity vs injection current.

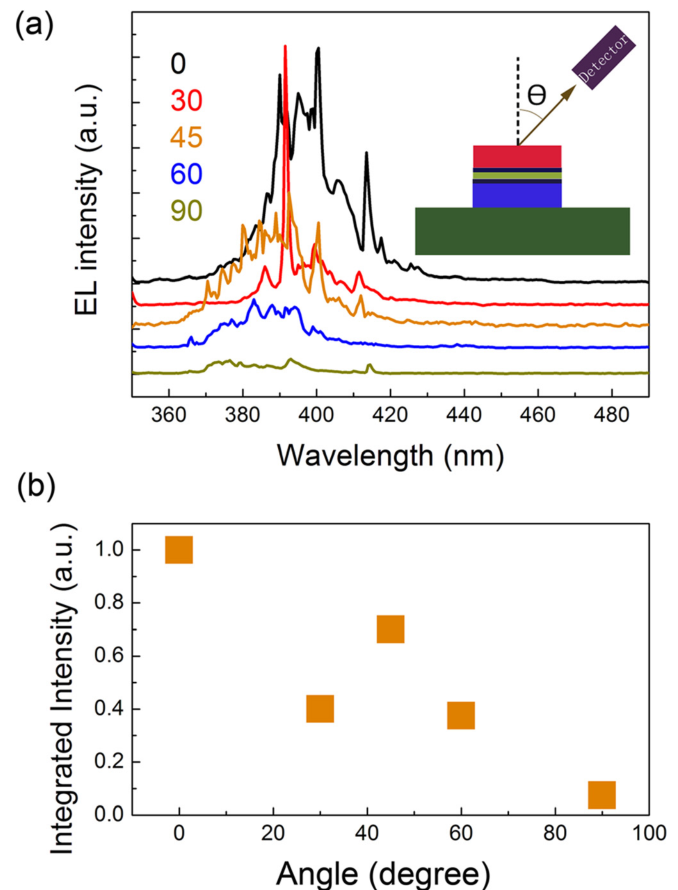

FIG. 5. (Color online) (a) EL spectra collected at different angles: 0°, 30°, 45°, 60°, and 90°, respectively. Inset: schematic of measurement angle. (b) Integrated spectrum intensity as a function of measurement angle.

Author complimentary copy. Redistribution subject to AIP license or copyright, see http://jap.aip.org/jap/copyright.jsp

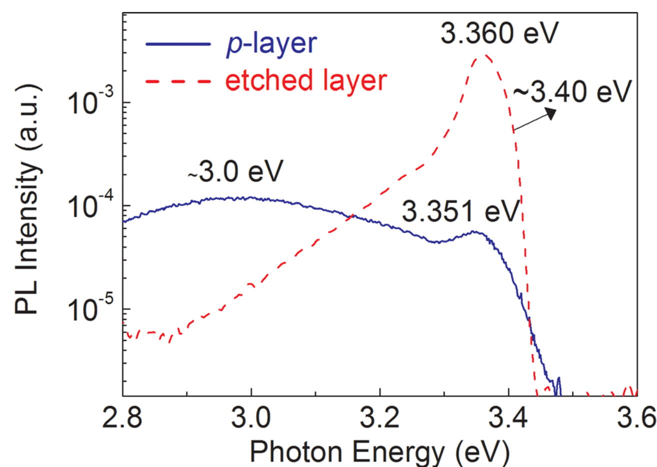

FIG. 6. (Color online) Low-temperature PL spectra from the top Sb-doped *p*-layer and the film with *p*-layer etched.

that there is a slight blueshift of the emission as the measurement angle increases. This trend is similar to the angle-dependent photoluminescence (PL) in ZnO columnar films grown by pulsed laser deposition,[19] which is mainly attributed to the effect of microcavity formed by the films.[20,21] The integrated intensity as a function of angle is shown in Fig. 5(b). This result is a typical far-field pattern characteristic of an LED; similar results were observed in GaN LEDs.[22]

In Sb–ZnO/Ga–ZnO homojunction LED, the light mostly arises from radiative recombination in Sb–ZnO layer.[12] Here, the enhanced emission power is a result of the carrier confinement and recombination in the MgZnO/ZnO/MgZnO double heterostructure. Figure 6 shows the low-temperature (9 K) PL spectra of the top *p*-type layer and the film with Sb-doped ZnO layer etched. The etching was done by using diluted HCl. The setup of the PL measurement is similar to the EL setup. A 325 nm He–Cd laser is used as the excitation source. As seen from the PL spectrum of the *p*-type layer, an acceptor-bound exciton emission (3.351 eV) and electron to zinc vacancy acceptor transition peak (~3.0 eV) can be observed, which is the signature of Sb-doped *p*-type ZnO.[8] The PL of the etched sample shows a donor bound exciton emission (3.360 eV) as well as a drastic increase of the PL intensity by almost two orders of magnitude, which originates from much better crystal quality of the undoped ZnO layer. There is a shoulder around 3.40 eV beside the main peak in the PL of the etched ZnO film, which is widely attributed to free exciton (*FX*) emission.[23] The presence of the *FX* peak is another strong proof of excellent optical quality of the undoped ZnO film. Under forward bias, radiative recombination happens in the undoped ZnO layer, rather than in the Sb-doped ZnO film, giving rise to the enhanced emission intensity.

IV. CONCLUSION

ZnO LEDs with Sb-doped *p*-ZnO, MgZnO/ZnO/MgZnO double heterostructure, *n*-ZnO were fabricated on *c*-plane sapphire using plasma-assisted MBE. The devices show prominent ultraviolet emission in the EL spectra. The output power of the LED was characterized to be 487 nW at the injection current of 140 mA thanks to the high crystalline quality of the intrinsic layer in the double heterostructure.

ACKNOWLEDGMENTS

The work on *p*-type materials was supported by DOE (Grant No. DE-FG02-08ER46520), and the work on devices was in part supported by ARO-YIP (Grant No. W911NF-08-1-0432) and by NSF (Grant No. EECS-0900978).

[1]D. C. Look, Mater. Sci. Eng. B **80**, 383 (2001).
[2]C. Klingshirm, J. Fallert, and H. Zhou, Phys. Status. Solidi. B **247**, 1424 (2010).
[3]A. Tsukazaki, A. Ohtomo, T. Onuma, M. Ohtani, T. Makino, M. Sumiya, K. Ohtami, S. F. Chichibu, S. Fuke, Y. Segawa, H. Ohno, H. Koinuma, and M. Kawasaki, Nat. Mater. **4**, 42 (2005).
[4]J. H. Lim, C. K. Kang, K. K. Kim, I. K. Park, D. K. Hwang, and S. J. Park, Adv. Mater. **18**, 2720 (2006).
[5]Y. R. Ryu, J. A. Lubguban, T. S. Lee, H. W. White, T. S. Jeong, C. J. Youn, and B. J. Kim, Appl. Phys. Lett. **90**, 131115 (2007).
[6]K. Nakahara, S. Akasaka, H. Yuji, K. Tamura, T. Fuji, Y. Nishimoto, D. Takamizu, A. Sakaki, T. Tanabe, H. Takasu, H. Amaike, T. Onuma, S. F. Chichibu, A. Tsukazaki, A. Ohtomo, and M. Kawasaki, Appl. Phys. Lett. **97**, 013501 (2010).
[7]S. Limpijumnong, S. B. Zhang, S. H. Wei, and C. H. Park, Phys. Rev. Lett. **92**, 155504 (2004).
[8]F. X. Xiu, Z. Yang, L. J. Mandalapu, D. T. Zhao, J. L. Liu, and W. P. Beyermann, Appl. Phys. Lett. **87**, 152101 (2005).
[9]L. J. Mandalapu, Z. Yang, F. X. Xiu, D. T. Zhao, and J. L. Liu, Appl. Phys. Lett. **88**, 092103 (2006).
[10]L. J. Mandalapu, F. X. Xiu, Z. Yang, and J. L. Liu, Appl. Phys. Lett. **88**, 112108 (2006).
[11]L. J. Mandalapu, Z. Yang, S. Chu, and J. L. Liu, Appl. Phys. Lett. **92**, 122101 (2008).
[12]S. Chu, L. J. Mandalapu, Z. Yang, and J. L. Liu, Appl. Phys. Lett. **92**, 152103 (2008).
[13]J. Y. Kong, S. Chu, M. Olmedo, and J. L. Liu, Appl. Phys. Lett. **93**, 132113 (2008).
[14]S. Chu, J. Y. Kong, M. Olmedo, Z. Yang, and J. L. Liu, Appl. Phys. Lett. **93**, 181106 (2008).
[15]Z. Yang, S. Chu, W. V. Chen, L. Li, J. Y. Kong, J. J. Ren, Paul K. L. Yu, and J. L. Liu, Appl. Phys. Express **3** 032101 (2010).
[16]J. W. Shin, J. Y. Lee, Y. S. No, T. W. Kim, and W. K. Choi, J. Appl. Phys. **100**, 013526 (2006).
[17]See supplementary material at http://dx.doi.org/10.1063/1.3598136 for C-V measurement and analysis.
[18]I. Schnitzer, E. Yablonovitch, C. Caneau, T. J. Gmitter, and A. Scherer, Appl. Phys. Lett. **63**, 2174 (1993).
[19]M. T. Taschuk, Y. W. Sun, and Y. Y. Tsui, Appl. Phys. A **90**, 141 (2008).
[20]N. Takada, T. Tsutsui, and S. Saito, Appl. Phys. Lett. **63**, 2032 (2003).
[21]S. Y. Huang, R. H. Horng, W. K. Wang, and D. S. Wuu, Phys. Status Solidi C **3**, 2137 (2006).
[22]M. F. Schubert, S. Chhajed, J. K. Kim, and E. F. Schubert, Appl. Phys. Lett. **91**, 051117 (2007).
[23]A. Teke, U. Ozgur, S. Dogan, X. Gu, and H. Morkoc, Phys. Rev. B **70**, 195207 (2004).

Author complimentary copy. Redistribution subject to AIP license or copyright, see http://jap.aip.org/jap/copyright.jsp